Proc. Natl. Acad. Sci. USA
Vol. 91, pp. 669–673, January 1994
Neurobiology

Waves and stimulus-modulated dynamics in an oscillating olfactory network

(*Limax maximus*/functional imaging/olfaction/propagation/temporal synchrony)

K. R. DELANEY*, A. GELPERIN, M. S. FEE, J. A. FLORES, R. GERVAIS†, D. W. TANK, AND D. KLEINFELD‡

AT&T Bell Laboratories, Murray Hill, NJ 07974

Communicated by John J. Hopfield, October 4, 1993 (received for review May 5, 1993)

ABSTRACT **The temporal dynamics of electrical activity in an olfactory organ, the procerebral lobe of the terrestrial mollusc *Limax maximus*, is studied. The lobe exhibits intrinsic oscillations in its field potential. Intracellular recordings show that the lobe contains two classes of neurons, both with activity phase-locked to the oscillation. Neurons in one class produce periodic bursts of spikes while those in the other class fire infrequently but receive strong, periodic inhibition whose onset coincides with the burst. The large-scale activity of these neurons is imaged in preparations stained with voltage-sensitive dyes. We observe waves of electrical activity that span the width of the lobe and travel its full length along a longitudinal axis. Simultaneous optical and intracellular recordings show that the form of the wave reflects the electrical activity of both classes of neurons. The application of natural odor stimuli causes the electrical activity along the lobe to transiently switch from the state with propagating waves to one with spatially uniform oscillations. The behavioral and computational relevance of this change in global timing is discussed.**

Rhythmic patterns of electrical activity are a ubiquitous feature of nervous systems (1). For circuits that contain relatively few neurons, such as those that control rhythmic motor patterns in invertebrates, the detailed dynamics and behavioral relevance of such activity are well characterized (2, 3). However, for extended circuits, such as those in cortical and subcortical areas that encompass hundreds or thousands of neurons, the detailed dynamics of oscillatory activity are poorly understood. Yet there is growing evidence to suggest that the modulation of oscillatory activity plays an essential role in the processing of sensory information (4, 5). In the olfactory bulb, this takes the form of odor-mediated changes in the strength and distribution of fast, spatially coherent oscillations (6, 7). In the mammalian visual system, this takes the form of stimulus-dependent changes in the temporal coherence of oscillatory activity between different locations in visual cortex (8, 9). This evidence provides strong motivation to visualize and understand the spatio-temporal structure of oscillatory dynamics in an extended network as well as the effects of natural stimuli and other perturbations on these dynamics.

Here we investigate the spatio-temporal dynamics of electrical activity in the procerebral (PC) lobe of the terrestrial mollusc *Limax maximus*. Several features support the choice of this preparation for the study of olfactory processing in an extended neuronal circuit. First, olfaction is the only sense available to *Limax* for perception at a distance. An acute olfactory sense enables *Limax* to forage successfully over distances of 10 or more meters in response to fluctuations in airborne odors (10). Odor can also be used to condition the behavior of *Limax* with a breadth and effectiveness that rivals the results associated with vertebrate species (11). Second, the PC lobe contains a relatively large number of neurons, $\approx 10^5$, that form extensive interconnections within cell-rich and neuropil-rich regions (12). Anatomical studies show that the lobe is the dominant recipient of afferent input from inferior and superior noses (13). Lastly, the local field potential (LFP) of the PC lobe oscillates continuously (13, 14). Oscillatory activity is also a salient feature of most vertebrate olfactory bulbs and the olfactory cortex of mammals (6, 7), although in vertebrates the oscillations are gated by inspiration.

We ask: What are the spatio-temporal patterns of electrical activity throughout the lobe? What is the relation between these patterns and the electrophysiology of the underlying neurons? What is the effect of odor on the patterns of activity? To answer these questions we make extensive use of optical imaging techniques in conjunction with dyes whose spectral properties are sensitive to membrane potential (V_m) (15, 16).

METHODS

Preparation. PC lobes are removed from 1- to 5-g animals that are hatched and raised in a controlled environment (17). For some optical measurements, lobes are embedded in 4% (wt/vol) low-melting point agarose (no. A-5030; Sigma) to reduce motion that arises from contraction of muscle that covers nerve trunks. In experiments that involve the application of odor, the nose (neuroepithelial pad of the superior tentacle) and olfactory nerve are isolated along with the lobe. The nose is maintained in an open but moist environment during the delivery of olfactory stimuli and is submerged between sets of stimuli. The electro-olfactogram is measured concomitant with each record. Stimuli consist of a pulse of air saturated with a dilute odorant or, as a control, water vapor. The volume of the pulse is 1 ml and is delivered over a period of 4 s through a large-bore multibarrel pipet placed within 1 mm of the sensory epithelium. The odorants include a component of natural potato odor, 10^{-5}% (vol/vol) 2-ethyl-3-methoxypyrazine (EMOP), and 10^{-4}% (vol/vol) of the filtered extract from freshly squeezed garlic cloves.

Optical Recording. We record voltage-dependent changes in the fluorescent yield of preparations stained with the dye di-4-ANEPPS (18) (no. D1199; Molecular Probes). The dye is prepared as a 1% (wt/vol) stock solution in 70% (vol/vol) ethanol/water and diluted to ≈0.002% (wt/vol) in isotonic

The publication costs of this article were defrayed in part by page charge payment. This article must therefore be hereby marked "*advertisement*" in accordance with 18 U.S.C. §1734 solely to indicate this fact.

Abbreviations: LFP, local field potential; EMOP, 2-ethyl-3-methoxypyrazine; PC, procerebral.

*Permanent address: Department of Biosciences, Simon Fraser University, Burnaby, BC V5A 1S6 Canada.
†Permanent address: Laboratoire de Physiologie Neurosensorielle, Centre National de la Recherche Scientifique, Universite Claude Bernard, Lyon 69622 Villeurbanne Cedex France.
‡To whom reprint requests should be addressed at: Room 1C-463, AT&T Bell Laboratories, 600 Mountain Avenue, Murray Hill, NJ 07974.

saline just before use. The preparation is stained at room temperature for at least 1 hr. The optical system is configured for epiillumination with a 546 ± 5 nm band-pass excitation filter (no. 546DF10; Omega Optical, Brattleboro, VT), a 580-nm dichroic mirror (no. 580 DRLP; Omega), and a 590-nm long-pass emission filter (no. OG590; Schott, Duryea, PA). The source is a 100-W quartz tungsten lamp (Xenophot HLX; Osram, Berlin). The power at the preparation is typically 5 μW. The emitted light is detected with either a small array of individual photodiodes (no. UV100; EG&G, Salem, MA) or a cooled charge-coupled device camera (model CH220; Photometrics, Tucson, AZ) situated at an image plane whose focus lies just below the surface of the preparation. The limiting source of noise in all measurements is photon statistics.

The average voltage change in the field of each detector or charged-coupled device element is linearly proportional to the fractional change in the measured emission—i.e., $\Delta V(x, y, t) \propto -\Delta F(x, y, t)/F(x, y)$, where $F(x, y, t)$ is the intensity of emitted light measured at time t by a detector whose field of view is centered at (x, y), $\Delta F(x, y, t) = F(x, y, t) - F(x, y)$, and $F(x, y) = (1/T)\Sigma_t F(x, y, t)$ with T equal to the number of frames in the sequence. Images of the change in potential inferred from the change in emission are presented as successive two-dimensional spatial maps of $-\Delta F/F$. The images are typically 100 × 100 pixels in size, spatially filtered by convolution with a 5 × 5 pixel triangular window and masked to exclude regions not occupied by the lobe. Different levels of voltage change are coded by false-color, with yellow/red indicating depolarization and blue/violet indicating hyperpolarization relative to the average potential.

RESULTS

PC lobes are symmetric protuberances from the cerebral ganglion. The cell layer of the lobe is most clearly discerned from the layer of neuropil when the isolated lobe is positioned on its side (Fig. 1*A*). Note how the cell layer forms the posterior face of the lobe and rolls around the tip that lies distal to the cerebral ganglion. The major part of the cell layer, except for those neurons that lie below the distal edge, is visible with the lobe positioned with the posterior face up (Fig. 1*B*). This orientation allows changes across the cell layer to be imaged and offers greater mechanical stability.

Electrophysiology of Individual Neurons. The characteristic intracellular waveforms of neurons across the posterior surface of the cell layer are surveyed. As the neurons are small, ≈6–8 μm in diameter, we typically make use of the perforated-patch recording technique (19). We also record the LFP in the vicinity of the patch electrode as a means to facilitate comparisons between cells. Two classes of intracellular responses, phase-locked to the oscillation, are observed (n = 77).

Neurons in one class, denoted bursting neurons, comprise about 10% of the sample and produce periodic bursts of action potentials (Fig. 2*A*). The period at room temperature is ≈1.4 s, as previously observed in the field potential (13). Several characteristic features are associated with the bursts.

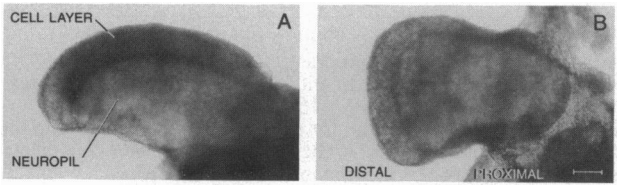

FIG. 1. Photomicrographs of the PC lobe. (*A*) Lateral view. (*B*) Posterior view. (Bar = 100 μm.)

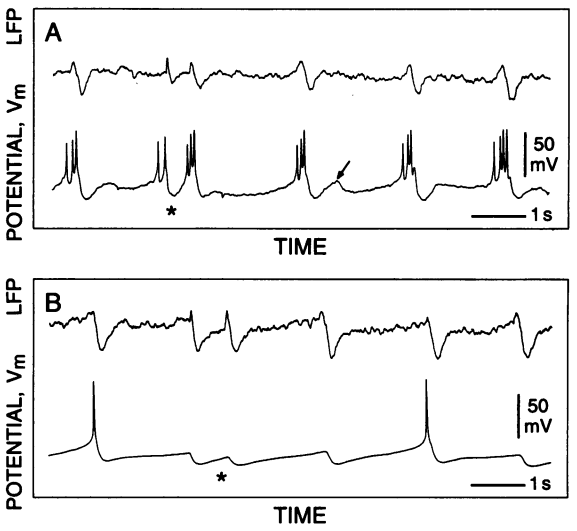

FIG. 2. Intracellular records and nearby LFP of the two classes of neurons that comprise the lobe. Temperature ≈ 18°C. (*A*) Perforated-patch record of a bursting neuron located in the middle of the lobe. (*B*) Perforated-patch record of a nonbursting neuron located, as above, in the middle of the lobe. Note the presence of double events (*) in both records.

(*i*) Each burst coincides with an event in the LFP. (*ii*) The instantaneous rate of firing within a burst tends to accelerate toward the end of a burst. (*iii*) The bursts are followed by a period of hyperpolarization and subsequently a depolarizing afterpotential (arrow, Fig. 2*A*). It is unclear to what extent the hyperpolarization is derived from synaptic input or represents a hyperpolarizing afterpotential. (*iv*) There is a small but significant chance for a second burst to occur after 0.2–0.4 s, concomitant with the depolarizing afterpotential, rather than after the normal period of ≈1.4 s. Such double bursts always coincide with rapid, double events in the LFP (* in Fig. 2*A*).

Neurons in the second class, denoted nonbursting neurons, are the major fraction of cells in the lobe and do not produce periodic bursts of action potentials. The characteristic features associated with these cells are as follows. (*i*) They receive strong, periodic inhibitory input (Fig. 2*B*) during every event in the LFP. (*ii*) The average rate of spiking is low, 0.5 spike per period, although some cells show as many as 6 spikes per period. (*iii*) Double events in the LFP appear as consecutive hyperpolarizations (* in Fig. 2*B*).

Large-Scale Electrical Behavior. Spatio-temporal maps of electrical activity are determined from optical images of the change in emission (n = 42). We observe a periodic wave of depolarization, followed by hyperpolarization, that travels along the axis of the preparation from the distal end toward the cerebral ganglion (Fig. 3 *A* and *C*). A lateral view shows that depolarization begins near the distal end of the lobe among cell somata and, concomitantly, within an anterior region of neuropil. The depolarization traverses the length of the cell layer, as shown by the distal to proximal progression of the red region in Fig. 3*A* (frames 6–10), until it ebbs. The spread in depolarization is followed by a similar spread in hyperpolarization (frames 9–11, Fig. 3*A*).

The detailed shape of the optical change as a function of time varies between different locations. Near the distal end of the lobe the change in emission appears sawtooth in shape (thick line, Fig. 3*B*), whereas toward the proximal end the waveform has a substantially sharper, spiked appearance (thin line, Fig. 3*B*). The maximum difference in temporal phase between proximal and distal regions varies between preparations but is relatively constant for a given lobe ($\Delta t \approx$ 0.2–0.5 s) at fixed temperature.

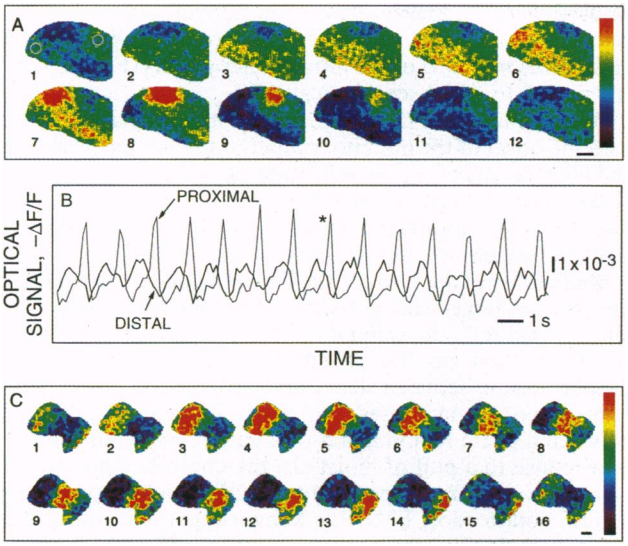

FIG. 3. Optical imaging of large-scale electrical activity across the PC lobe. (*A*) Lateral view (Fig. 1*A*) of the optically detected voltage signal, $-\Delta F/F$, plotted as successive frames to show spatially resolved changes in emission. Temperature = 18°C. Imaging parameters: 120 ms per frame and $-\Delta F/F$(full scale) = -2.5×10^{-3} (violet or hyperpolarization) to $+2.5 \times 10^{-3}$ (red or depolarization). (*B*) Optical signal versus time for distinct distal (thick line) and proximal (thin line) locations in the lobe. Each signal is the average response from the circled regions in *A*. The asterisk (*) corresponds to frame 8 in *A*. (*C*) Posterior view (Fig. 1*B*). Temperature = 14°C. Parameters: 112 ms per frame and $-\Delta F/F$(full scale) = $\pm 1.5 \times 10^{-3}$. (Bars = 100 μm.)

When the top of the cell layer is observed in a posterior exposure (Fig. 1*B*), a band of depolarization begins at the distal tip and moves proximal along the length of the lobe (Fig. 3*C*). The band of depolarization is followed by a band of hyperpolarization, consistent with the pattern of activity observed in the cell layer as viewed in a lateral exposure (Fig. 3*A*). Under optimal conditions, activity is seen to propagate past the cell layer and slightly into the cerebral ganglion before it ebbs (Fig. 3*C*). A posterior exposure of the preparation offers mechanical stability that is crucial for experiments with odor stimuli, but the full extent of the timing difference between distal and proximal ends is often less pronounced because of the substantial overlap of cells at the distal end (e.g., see Fig. 6).

The state with periodic, propagating waves (Fig. 3) is the dominant pattern of electrical behavior of the lobe. However, as discussed in the context of the intracellular records (Fig. 2), the rhythmic pattern of activity is occasionally interrupted by double events. We image the electrical activity of the lobe prior to and during these events to ascertain if they modify the propagation of waves across the lobe. Normal propagation is observed prior to the double event (frames 1–14 in Fig. 4) but a transient collapse of the phase difference between the distal and proximal regions of the lobe occurs during the first of the pair of bursts (frame 19 in Fig. 4). The phase gradient is partially reestablished by the second burst (frames 22–25 in Fig. 4), after which the normal pattern of activity resumes. This behavior is seen in isolated lobes (n = 5) and in preparations with the nose attached (n = 3). These data show that the lobe transiently supports a spatially uniform state in addition to the normal propagating state.

Relation Between Optical and Electrical Signals. The signal measured by a given photodetector is a spatial average of the changes in intracellular potential of all neurons present in the volume that contributes emitted light to that photodetector. *A priori*, it is possible that the appearance of waves in the optical signal reflects a spatial gradient of activity in neurons

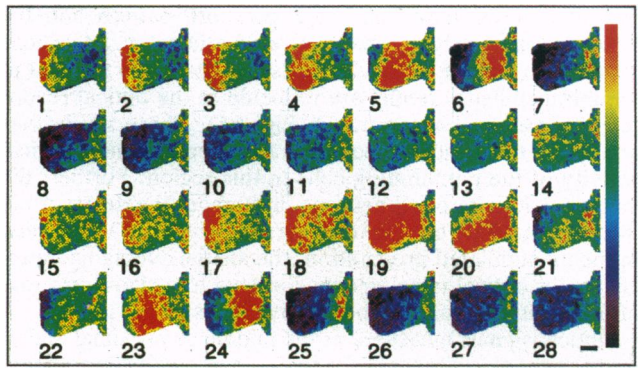

FIG. 4. Optically recorded electrical activity before and during a double event. Posterior view, plotted as successive images. Temperature = 18°C. Parameters: 112 ms per frame and $-\Delta F/F$(full scale) = $\pm 1.8 \times 10^{-3}$. (Bar = 100 μm.)

with different waveforms, rather than a temporal gradient of activity across neurons in the lobe. Thus we seek to relate the electrophysiological properties of neurons in the lobe to the observed optical signal as a means to interpret the origin of the propagating waves.

The presence of only two classes of neurons in the lobe suggests that we should be able to interpret our optical signals in terms of the intracellular potentials of these neurons. We first consider simultaneous measurements of the intracellular potential in nonbursting neurons and the optical signal in the field that encompasses the cell. For neurons situated near the distal tip (Figs. 1*B* and 3*A*), the oscillations in electrical and

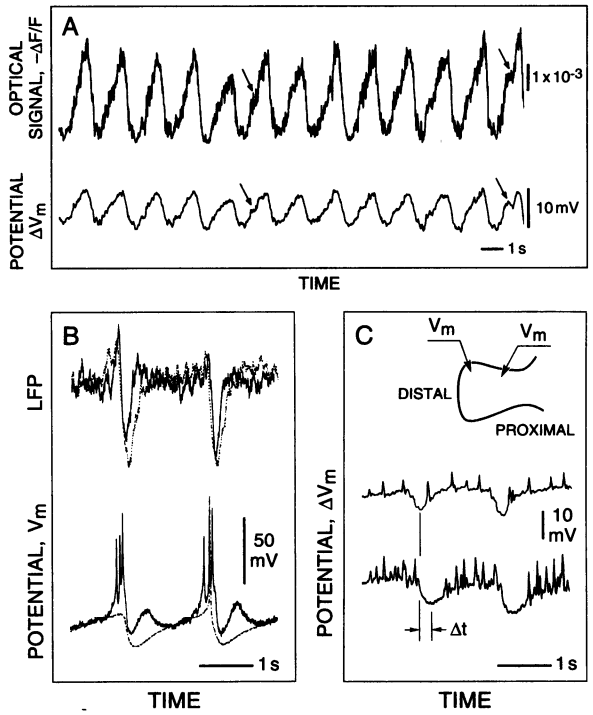

FIG. 5. Relation of different signals from the lobe. (*A*) Simultaneous intracellular and optical recordings at the distal end of the lobe. The lower trace is the whole-cell patch record of a nonbursting cell and the upper trace is the photodiode signal from a 50-μm (diameter) region surrounding the patch electrode tip. Temperature ≃ 18°C. (*B*) Relative timing between the output from a bursting and a nonbursting neuron (Fig. 2). The traces were aligned by shifting the time base of one record so that the leading edges of the two LFPs coincided. (*C*) Simultaneous whole-cell patch records from two nonbursting neurons. The fast events are spikes, low-pass filtered at 30 Hz, that result from leakage currents. Temperature ≃ 18°C.

optical records show the same sawtooth pattern and the signals are perfectly in phase with each other (Fig. 5*A*). Close examination of the records reveals that even fine features in the intracellular potential are reflected in the optical record (e.g., corresponding arrows in Fig. 5*A*). These similarities imply that the optical signal accurately reports the electrical activity of the nonbursting cells in this region. Further, the electrical activity of all neurons throughout the depth of the field, estimated to be $\approx 10^3$ cells, is strongly correlated. Thus, in the unstimulated preparation, the spatial averaging inherent in our optical imaging does not lead to a significant loss of information about the neural dynamics in the lobe.

Optical signals measured at the middle or proximal end of the lobe are also similar in shape to the intracellular potential measured from nonbursting neurons at the same locations, with the exception that the optical signals have a peak (Fig. 3*B*) just prior to the onset of hyperpolarization. A line of evidence shows that the timing of the peak in the optical record is consistent with the timing of the depolarization seen in the intracellular records. The peak intracellular depolarization in bursting (Fig. 2*A*) and nonbursting neurons (Fig. 2*B*) occurs just prior to the onset of hyperpolarization. Further, the depolarizing events in both classes of neurons are coincident, as determined by aligning the LFPs from simultaneous measurements of intracellular potential and the nearby LFP in separate experiments (Fig. 5*B*). The relatively small amplitude of the peak is consistent with the apparently small fraction of bursting cells in the lobe and with the relatively low rate of firing by nonbursting cells.

The presence of propagating waves in the optical images (Fig. 3) implies that there is a phase lag between changes in intracellular potential of neurons at opposite ends of the lobe. To check for this difference in timing, we made simultaneous whole-cell patch measurements on nonbursting neurons at nearly opposite ends of the cell layer ($n = 6$). We observe differences in timing of the intracellular signals (Fig. 5*C*) that are similar to those seen optically.

We conclude that the peak of the optical signal coincides with the onset of the inhibitory input to the nonbursting cells and with the end of the burst in bursting cells. Thus the waves observed in the optical signal correspond to waves of subthreshold and suprathreshold intracellular activity that propagate across all neurons in the lobe.

Modulation of the Wave with Natural Stimuli. We return to the issue of large-scale activity in the lobe and address the effect of natural odor stimuli delivered to the exposed nose. We focus first on the difference in timing of the peak depolarization between distal and proximal regions of the preparation, as measured optically. The phase difference between a distal region and a proximal region is unchanged in response to a puff of moist air, the control stimulus (Fig. 6*A*). However, in response to a puff of a component of natural potato odor, EMOP, a known appetitive stimulus to naive animals (20), the change in phase difference between distal and proximal regions is dramatic. The response of the lobe on its first exposure to the odorant is shown in Fig. 6*B*. The stimulus leads to a collapse of the phase difference between the distal and proximal regions—i.e., an initial difference of $\Delta t \gtrsim 250$ ms is reduced to $\Delta t < 50$ ms. Further, with this initial application there is a transient increase in the instantaneous frequency that appears to arise from extra bursts that occur during double events (Fig. 4). Wave propagation, equivalent to that observed before the stimulus, resumes about 10 periods after cessation of the odor.

The change in relative timing in response to odorant is robust. Repeated exposure of the preparation to odorant

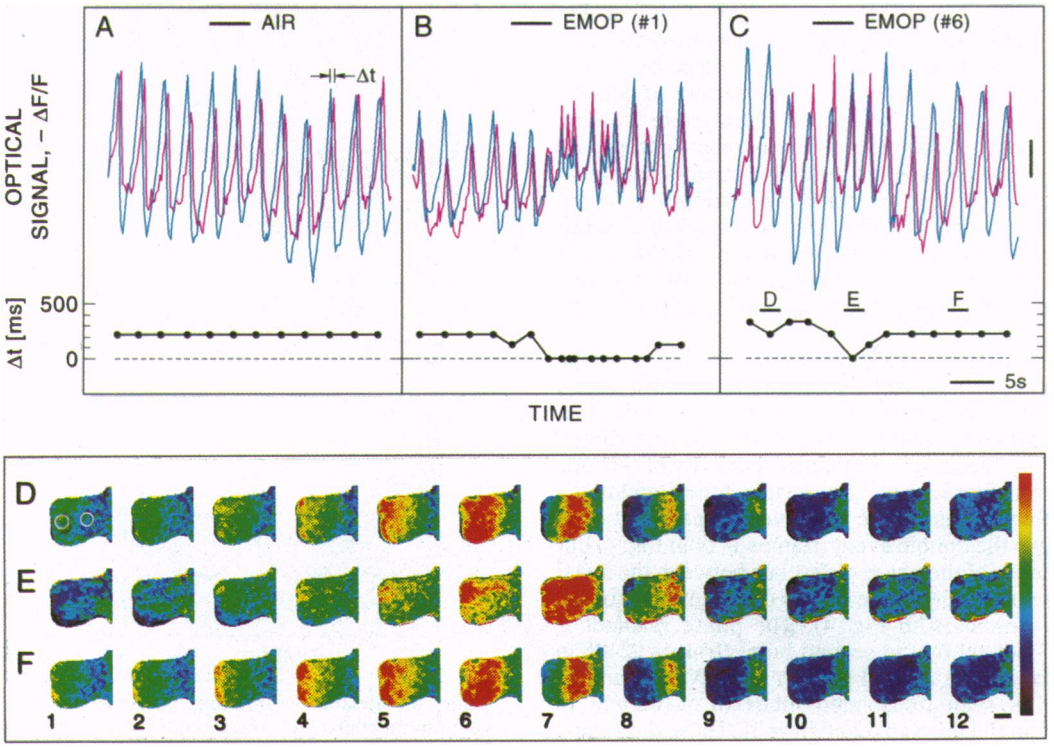

FIG. 6. Optically recorded electrical activity across the lobe in response to natural odor stimuli. The same preparation is used throughout. Temperature = 14°C. (*A*) Average change in emission, $-\Delta F/F$, versus time during the exposure of the preparation to moist air. The change is shown for distal (blue line) and proximal (red line) regions, as delineated by the circled regions in *D*. The bar marks the delivery of the stimulus. The lower plot shows the time between successive peaks in the optical signal, Δt, for each period. (*B*) Average change in emission versus time during the first exposure of the preparation to EMOP. (*C*) Average change in emission during the sixth exposure to EMOP. The letters D–F correspond to periods shown as successive optical images in *D*–*F*. (*D*–*F*) Images corresponding to the data in *C*. The subsequences are taken prior to (*D*), during (*E*), and after (*F*) stimulation of the nose with EMOP. Parameters: 112 ms per frame and $-\Delta F/F$(full scale) = $\pm 2.5 \times 10^{-3}$. (Bar = 100 μm.)

leads to a collapse of the phase difference between proximal and distal regions, although there is a faster recovery of wave propagation. The response to EMOP on the sixth set of stimuli is shown in Fig. 6*C*, for which full synchrony occurs for one period. Note that the synchronous period is not attended by a transient increase in frequency or the appearance of double events, as observed after the first exposure to odorant. Changes in the phase similar to that shown in Fig. 6 *A* and *C* are seen in all preparations for which the electro-olfactogram demonstrated that the neuroepithelium was responsive during the presentation of odor ($n = 25$); $\Delta t = 310 \pm 90$ ms (mean ± standard deviation) prior to stimulation and $\Delta t = 50 \pm 50$ ms following stimulation. We observe a similar collapse of the phase gradient following delivery of garlic odor, a natural aversive odorant for *Limax*.

We now focus on the spatial distribution of electrical activity in the lobe prior to, during, and after the presentation of odor (Fig. 6*C*). Compared to measurements made in the absence of stimulation, the fidelity of our images is compromised by motion of the preparation. Movements are caused by contractions in the olfactory nerve that are exacerbated by application of odor to the nose. Prior to stimulation, we observe the normal propagation of bands of depolarization activity across the posterior face of the lobe prior to stimulation (Fig. 6*D*). Following the presentation of EMOP, we observe relatively brief epochs of depolarization during each cycle (Fig. 6*E*). The depolarizing epochs span the extent of the lobe (frame 7, Fig. 6*E*) and correspond to the collapse of the phase difference across the lobe (Fig. 6*C*). Wave propagation, similar to that observed before the stimulus, resumes following cessation of the odor (Fig. 6*F*).

DISCUSSION

The optical methods employed here have allowed us to identify waves of electrical activity that propagate across the entire surface of the PC lobe, the central olfactory network of *Limax*. Although the network in *Limax* may be especially well suited for uncovering large-scale spatio-temporal patterns of activity, it is likely that analogous patterns are present in other systems. In particular, extensive studies of the field potential at multiple sites in mammalian bulb show that there are defined spatial patterns of variation in the amplitude of the oscillation across the bulb (21). Further, there is limited evidence for phase shifts across the bulb (22). It may be useful to reinvestigate the spatio-temporal patterns of activity in the bulb with imaging techniques similar to those employed in the present work.

The relative phase of oscillatory activity across the lobe is transiently and dramatically reduced by odor stimuli (Fig. 6). The collapse of the phase gradient in activity can occur without a significant change in the waveform and frequency of the oscillations (Fig. 6*C*). Though details of the circuitry within the lobe are largely unknown, analogies between the dynamics reported here and theoretical understanding of excitable media (23) suggest that the phase gradient originates from a spatial gradient of excitability across the lobe. In the absence of external stimuli the gradient of excitability is such that the wavelength of the oscillating activity is roughly the size of the lobe (Fig. 3). Odor stimuli (Fig. 6) or double events (Fig. 4) reduce the gradient but do not necessarily change the average level of excitability, so that the wavelength becomes long compared to the size of the lobe. This results in the transient appearance of spatially uniform oscillations. The spatial collapse of the gradient during double events (Fig. 4) suggests that the normal activity of the lobe may be poised close to a transition between the propagating and synchronous states.

The spatially synchronous state in the PC lobe is likely to correspond to a global aspect of behavior, such as a change in attentiveness of the animal to its olfactory environment. Within this hypothesis, the reduction in phase that occurs during spontaneous double events in *Limax* (Fig. 4) is a consequence of the sensitivity of the network to weak olfactory stimuli and results in spontaneous sampling of the environment. Analogous changes in global synchrony occur in visual (24) and motor (25) areas of mammalian cortex during periods of attention. Beyond issues of attention, a spatially synchronous state may gate synaptic plasticity within the lobe. Indeed, plasticity within mammalian hippocampus (26) and olfactory cortex (4) depends on near-synchronous timing between synaptic pathways.

We thank B. I. Shraiman and H. Sompolinsky for discussions that shaped the direction of this work. We also thank T. H. Bullock, L. B. Cohen, B. Friedman, J. J. Hopfield, and H. S. Seung for valuable criticism, W. Denk for advice on optics, T. Kovacs and R. A. Stepnoski for assistance with software, and K. Kimmick for animal care. K.R.D. was supported by a postgraduate fellowship from the Medical Research Council of Canada and by a grant from the National Sciences and Engineering Research Council. D.K. acknowledges support from the U.S.–Israel Binational Science Foundation.

1. Basar, E. & Bullock, T. H., eds. (1992) *Induced Rhythms in the Brain* (Birkhäuser, Boston).
2. Getting, P. A. (1989) *Annu. Rev. Neurosci.* **12,** 185–204.
3. Kleinfeld, D. & Sompolinsky, H. (1989) in *Methods in Neuronal Modeling: From Synapses to Networks*, eds. Koch, C. & Segev, I. (MIT Press, Cambridge, MA), pp. 195–246.
4. Ketchum, K. L. & Haberly, L. B. (1991) in *Olfaction: A Model System for Computational Neuroscience*, eds. Davis, J. L. & Eichenbaum, H. (MIT Press, Cambridge, MA), pp. 69–100.
5. Schuster, H. G., ed. (1991) *Nonlinear Dynamics and Neuronal Networks: Proceedings of the 63rd W. E. Heraues Seminar, Friedrichsdorf 1990* (VCH, New York).
6. Adrian, E. D. (1941) *J. Physiol. (London)* **100,** 459–473.
7. Freeman, W. (1975) *Mass Action in the Brain* (Academic, New York).
8. Eckhorn, R., Bauer, R., Jordan, W., Brosch, M., Kruse, W., Munk, M. & Reiboeck, R. J. (1988) *Biol. Cybern.* **60,** 121–130.
9. Gray, C. M., Konig, P., Engel, A. K. & Singer, W. (1989) *Nature (London)* **338,** 334–337.
10. Gelperin, A. (1974) *Proc. Natl. Acad. Sci. USA* **71,** 966–970.
11. Sahley, C. L. (1990) in *Connectionist Modeling and Brain Function: The Developing Interface*, eds. Hanson, S. & Olson, C. (MIT Press, Cambridge, MA), pp. 36–73.
12. Chase, R. & Tolloczko, B. (1993) *Micro. Res. Tech.* **24,** 214–230.
13. Gelperin, A., Rhines, L. D., Flores, J. & Tank, D. W. (1993) *J. Neurophysiol.* **69,** 1930–1939.
14. Gelperin, A. & Tank, D. W. (1990) *Nature (London)* **345,** 437–440.
15. Orbach, H. S. & Cohen, L. B. (1983) *J. Neurosci.* **3,** 2251–2262.
16. Kauer, J. S. (1988) *Nature (London)* **331,** 166–168.
17. Wieland, S. J. & Gelperin, A. (1983) *J. Neurosci.* **3,** 1735–1745.
18. Fluhler, E., Burnham, V. G. & Loew, L. M. (1985) *Biochemistry* **24,** 5749–5755.
19. Horn, R. & Marty, A. (1988) *J. Gen. Physiol.* **92,** 145–159.
20. Hopfield, J. F. & Gelperin, A. (1989) *Behav. Neurosci.* **103,** 274–293.
21. Freeman, W. J. & Baird, B. (1987) *Behav. Neurosci.* **101,** 393–408.
22. Freeman, W. J. (1978) *Electroencephalogr. Clin. Neurophysiol.* **44,** 586–605.
23. Murray, J. D. (1989) *Mathematical Biology* (Springer, Berlin).
24. Bouyer, J. J., Montaron, M. F. & Rougeul, A. (1981) *Electroencephalogr. Clin. Neurophysiol.* **51,** 244–252.
25. Murthy, V. N. & Fetz, E. E. (1992) *Proc. Natl. Acad. Sci. USA* **89,** 5670–5674.
26. Stewart, O., White, G., Korol, D. & Levy, W. B. (1988) in *Long-Term Potentiation: From Biophysics to Behavior*, eds. Landfield, P. W. & Deadwyler, S. A. (Liss, New York), pp. 139–166.